
VERIX: Towards Verified Explainability of Deep Neural Networks

Min Wu, Haoze Wu, Clark Barrett

Department of Computer Science, Stanford University
 {minwu, haozewu, barrett}@cs.stanford.edu

Abstract

We present VERIX, a system for producing *optimal robust explanations* and generating *counterfactuals* along decision boundaries of machine learning models. We build such explanations and counterfactuals iteratively using constraint solving techniques and a heuristic based on feature-level sensitivity ranking. We evaluate our method on image recognition benchmarks and a real-world scenario of autonomous aircraft taxiing.

1. Introduction

Broad deployment of artificial intelligence (AI) systems in safety-critical domains, such as autonomous driving (Grigorescu et al., 2020) and healthcare (Yu et al., 2018), necessitates the development of approaches for trustworthy AI. One key ingredient for trustworthiness is *explainability*: the ability for an AI system to communicate the reasons for its behavior in terms that humans can understand.

Early work on explainable AI includes well-known model-agnostic explainers which produce explanations that remain valid for nearby inputs in feature space. In particular, LIME (Ribeiro et al., 2016) and SHAP (Lundberg & Lee, 2017) learn simple, and thus interpretable, models locally around a given input. Following LIME, work on Anchors (Ribeiro et al., 2018) attempts to identify a subset of such input explanations that are (almost) sufficient to ensure the corresponding output value. However, such approaches are heuristic and do not provide any formal guarantees. They are thus inappropriate for use in high-risk scenarios. For instance, if a loan application model used by a bank has an explanation claiming that it depends only on a user’s “age”, “employment type” and “salary range”, yet in actuality, applicants with the same such attributes but different “gender” or “ethnicity” receive dissimilar loan decisions, then the explanation is not only wrong, but may actually mask bias in the model. Another drawback of model-agnostic approaches is that they often depend on access to training data, which may not always be available (perhaps due to privacy concerns). And even if available,

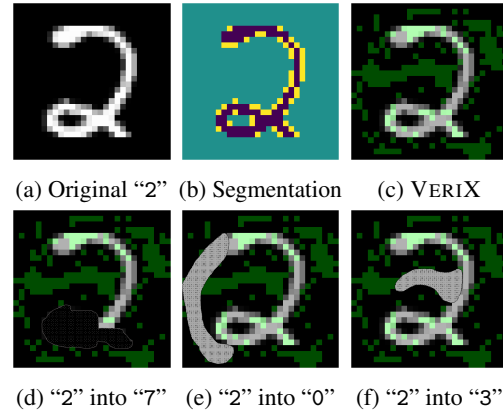


Figure 1. Intuition for our VERIX approach: (a) An MNIST handwritten “2”; (b) Segmentation of “2” into 3 partitions; (c) VERIX explanation (green pixels) of “2”; (d)(e)(f) Masking white pixels or whitening black pixels may turn “2” into possible counterfactuals.

distribution shift can compromise the results.

Recent efforts towards *formal* explainable AI (Marques-Silva & Ignatiev, 2022) aim to compute rigorously defined explanations that can guarantee *soundness*, in the sense that fixing certain input features is sufficient to ensure the invariance of a model’s prediction. However, their work only considers *unbounded* perturbations, which may be too course-grained to be useful (for other limitations, see Section 5). To mitigate those drawbacks, (La Malfa et al., 2021) bring in two types of *bounded* perturbations, ϵ -ball and k -NN box closure, and show how to compute *optimal robust explanations* with respect to these perturbations for natural language processing (NLP) models. k -NN box closure essentially chooses a finite set of the k closest tokens for each word in a text sample, so the perturbation space is intrinsically discrete; on the other hand, ϵ -ball perturbations provide a way to handle a continuous word embedding (though the authors of (La Malfa et al., 2021) suggest that these may be more cumbersome in NLP applications and focus on k -NN box perturbations in their experimental results).

In this paper, we present VERIX (VERIFIED explainability), a tool for computing *optimal robust explanations* (OREs) in the style of (La Malfa et al., 2021). Our work expands

on theirs in four important ways: (i) we focus on ϵ -ball perturbations and perception models, whose characteristics and challenges are different from those of NLP models; (ii) whereas (La Malfa et al., 2021) simply points to existing work on hitting sets and minimum satisfying assignments for computing OREs, we provide a detailed algorithm with several illustrative examples, and include a concrete traversal heuristic that performs well in practice; we believe these details are useful for anyone wanting to produce a working implementation; (iii) we note for the first time the relationship between OREs and counterfactual explanations; and (iv) we provide an extensive evaluation on a variety of perception models. We also note that in some aspects, our work is more limited: in particular, we use a simpler definition of ORE (without a cost function) as our algorithm is specialized for the case of finding explanations with the fewest features.

We start by providing intuition for our VERIX approach by analyzing an example explanation in Figure 1. The original MNIST digit “2” is shown in Figure 1a. Anchors (Ribeiro et al., 2018), mentioned above, relies on partitioning an image into a disjoint set of segments and then selecting the most prominent segment(s). Figure 1b shows “2” divided into 3 parts using k-means clustering (Lloyd, 1982). Based on this segmentation, the purple and yellow parts would be chosen for the explanation, suggesting that the model largely relies on these pixels to make its decision. This also matches our intuition, as a human would immediately identify these pixels as containing information and disregard the background. However, does this mean it is enough to focus on the salient features when explaining a classifier’s prediction? Not necessarily. VERIX’s explanation is highlighted in green in Figure 1c. It demonstrates that *whatever is prominent is important but what is absent in the background also matters*. We observe that VERIX not only marks those white pixels forming the silhouette of “2” but also includes some background pixels that might affect the prediction if changed. For instance, neglecting the bottom white pixels may lead to a misclassification as a “7”; meanwhile, the classifier also needs to check if the pixels along the left and in the middle are not white to make sure it is not “0” or “3”. While Figures 1d, 1e, and 1f are simply illustrative to provide intuition about why different parts of the explanation may be present, we remark that explanations from VERIX are produced automatically and deterministically.

2. VERIX: Verified Explainability

Let \mathcal{N} be a neural network and \mathbf{x} a d -dimensional input vector of features $\langle \chi^1, \dots, \chi^d \rangle$. We use $\Theta(\mathbf{x})$, or simply Θ , when the context is clear, to denote its set of feature indices $\{1, \dots, d\}$. We write $\mathbf{x}^{\mathbf{A}}$ where $\mathbf{A} \subseteq \Theta(\mathbf{x})$ to

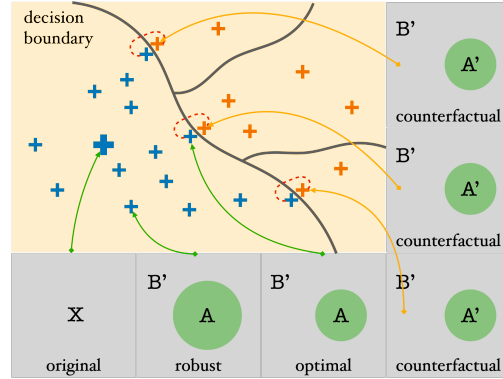


Figure 2. Graphical illustration of VERIX. Each gray square represents the original input \mathbf{x} (big blue “+”) or its variant (smaller “+”). Variants (blue “+”) that do not change the explanation \mathbf{A} (green circle) are guaranteed to lie on the same side of the decision boundary. Counterfactuals (orange “+”) with perturbed explanations \mathbf{A}' and irrelevant features are classified differently.

denote only those features indexed by indices in \mathbf{A} . We denote model prediction as $\mathcal{N}(\mathbf{x}) = c$, where c is a single quantity in regression or a label among others ($c \in C$) in classification. For the latter, we use $\mathcal{N}_c(\mathbf{x})$ to denote the confidence value (pre- or post- softmax) of classifying as c , i.e., $\mathcal{N}(\mathbf{x}) = \arg \max \mathcal{N}_c(\mathbf{x})$. Depending on different application domains, \mathbf{x} can be an image consisting of d pixels as in our case or a text comprising d words as in NLP (La Malfa et al., 2021). In this paper, we focus on perception models. This has the additional benefit that explanations in this context are self-illustrative and thus easier to understand.

2.1. Optimal Robust Explanations

Existing work such as abductive explanations (Ignatiev et al., 2019), prime implicants (Shih et al., 2018), and sufficient reasons (Darwiche & Hirth, 2020) define a formal explanation as a minimal subset of input features that are responsible for a model’s decision, in the sense that *any possible* perturbations on the rest features will *never* change prediction. Building on this, (La Malfa et al., 2021) introduces *bounded* perturbations and computes *optimal robust explanations* for NLP models. Our definition closely follows (La Malfa et al., 2021) except: (1) rather than minimizing an arbitrary cost function, we consider the uniform case as to compute the smallest number of features; (2) we focus on ϵ -ball perturbations not k -NN box closure; (3) we allow for bounded variation (parameterized by δ) in the output to accommodate both classification (set δ to 0) and regression (δ could be some pre-defined hyper-parameter quantifying the allowable output change) whilst (La Malfa et al., 2021) focuses on sentiment analysis (i.e., binary classification).

Definition 2.1 (Optimal Robust Explanation). Given a network \mathcal{N} , an input \mathbf{x} , a manipulation magnitude ϵ , and a discrepancy δ , a *robust explanation* with respect to norm

$p \in \{1, 2, \infty\}$ is a set of input features \mathbf{x}^A such that if $\mathbf{B} = \Theta(\mathbf{x}) \setminus \mathbf{A}$, then

$$\forall \mathbf{x}^{B'}. \left\| \mathbf{x}^B - \mathbf{x}^{B'} \right\|_p \leq \epsilon \Rightarrow |\mathcal{N}(\mathbf{x}) - \mathcal{N}(\mathbf{x}')| \leq \delta, \quad (1)$$

where $\mathbf{x}^{B'}$ is some perturbation on features \mathbf{x}^B and \mathbf{x}' is the input variant combining \mathbf{x}^A and $\mathbf{x}^{B'}$. In particular, we say that the robust explanation \mathbf{x}^A is *optimal* if

$$\begin{aligned} \forall \chi \in \mathbf{x}^A. \exists \mathbf{x}^{B'}, \chi'. \left\| (\mathbf{x}^B \oplus \chi) - (\mathbf{x}^{B'} \oplus \chi') \right\|_p \leq \epsilon \\ \wedge |\mathcal{N}(\mathbf{x}) - \mathcal{N}(\mathbf{x}')| > \delta, \quad (2) \end{aligned}$$

where χ' is some perturbation of χ and \oplus denotes concatenation of two features.

We refer to \mathbf{x}^B as the *irrelevant* features. Intuitively, perturbations bounded by ϵ imposed upon the irrelevant features \mathbf{x}^B will *never* change prediction, as shown by the small blue “+” variants in Figure 2. Moreover, each feature χ (and their combinations) in the optimal explanation \mathbf{x}^A can be perturbed, together with the irrelevant features, to go beyond the decision boundary, i.e., the orange “+” variants. We mention two special cases: (1) if \mathbf{x} is ϵ -robust, then all features are irrelevant, i.e., $\mathbf{A} = \emptyset$, meaning there is no valid explanation as any ϵ -perturbation does not affect the prediction at all (in other words, a larger ϵ is required to get a meaningful explanation); (2) if perturbing any feature in input \mathbf{x} can change the prediction, then $\mathbf{A} = \Theta(\mathbf{x})$, meaning the entire input is an explanation.

We remark that our definition of optimality is *local* in that it computes a *minimal* subset of features. An interesting problem would be to find a *globally optimal* explanation, i.e., the smallest (fewest features) among all possible local optima, also known as the cardinality-minimal explanation (Ignatiev et al., 2019). Approaches (such as those based on minimum hitting sets (La Malfa et al., 2021; Bassan & Katz, 2022)) for computing such global optima are often too computationally difficult to converge for large models and high-dimensional inputs as in our case. Therefore, we propose a tractable heuristic (Section 3.3) that approximates the ideal and works fairly well in practice.

2.2. Counterfactuals Along Decision Boundary

While there are infinitely many variants in the input space, we are particularly interested in those that lie along the decision boundary of a model. Figure 2 shows several pairs of variants (blue and orange “+”) connected by red dotted lines. Each pair has the property that the blue variant produces the same prediction as the original input \mathbf{x} , whereas the orange variant, obtained by further perturbing *only one* feature χ in the optimal explanation \mathbf{x}^A (together with the irrelevant features, i.e., $\mathbf{x}^{B'} \oplus \chi'$ in Equation (2) of Definition 2.1), produces a different prediction. We note that

Figure 3. Computing a VERIX explanation by constraint solving for a simple input $\mathbf{x} = \langle \chi^1, \dots, \chi^9 \rangle$. Green is the *optimal robust explanation* \mathbf{x}^A ; gray denotes irrelevant features \mathbf{x}^B .

these orange variants are essentially *counterfactual* explanations (Wachter et al., 2017): each is a concrete example of a nearby point in the input space illustrating one way to change the model prediction. We emphasize that our focus in this paper is to compute OREs, but it is noteworthy that these counterfactuals are generated automatically and at no additional cost during the computation of the ORE. In fact, we end up with a distinct counterfactual explanation for each feature in the ORE, as we will see below (see (Verma et al., 2020) for a comprehensive review of counterfactual explanations and their uses).

3. Computing VERIX Explanations by Constraint Solving

Before presenting the VERIX algorithm (Algorithm 1) in detail, we first illustrate it via a simple example.

Example 3.1 (VERIX Computation). Suppose \mathbf{x} is an input with 9 features $\langle \chi^1, \dots, \chi^9 \rangle$ as in Figure 3, and we have classification network \mathcal{N} , a perturbation magnitude ϵ , and are using $p = \infty$. The outer loop of the algorithm traverses the input features. For simplicity, assume the order of the traversal is from χ^1 to χ^9 . Both the explanation index set \mathbf{A} and the irrelevant set \mathbf{B} are initialized to \emptyset . At each iteration, VERIX decides whether to add the index i to \mathbf{A} or \mathbf{B} . The evolution of the index sets is shown in Table 1. Concretely, when $i = 1$, VERIX formulates a *pre-condition* which specifies that χ^1 can be perturbed by ϵ while the other features remain unchanged. An automated reasoner is then invoked to check whether the pre-condition logically implies the *post-condition* (in this case, $\mathcal{N}(\mathbf{x}) = \mathcal{N}(\hat{\mathbf{x}})$, meaning the prediction is the same after perturbation). Suppose the reasoner returns True; then, no ϵ -perturbation on χ^1 can alter the prediction. Following Equation (1) of Definition 2.1, we thus add χ^1 to the irrelevant features \mathbf{x}^B . Figure 3, top left, shows a visualization of this. VERIX next moves on to χ^2 . This time the precondition allows ϵ -perturbations on both χ^1 and χ^2 while keeping the other features unchanged.

Table 1. Evolving constraints and optimal explanation \mathbf{x}^A along reasoning result (True/False) when processing Example 3.1.

feature	A	B	B'	reasoner	irrelevant features \mathbf{x}^B	explanation \mathbf{x}^A
χ^1	\emptyset	\emptyset	$\mathbf{B} \cup \{1\}$	True	$\langle \chi^1 \rangle$	–
χ^2	\emptyset	$\{1\}$	$\mathbf{B} \cup \{2\}$	True	$\langle \chi^1, \chi^2 \rangle$	–
χ^3	\emptyset	$\{1, 2\}$	$\mathbf{B} \cup \{3\}$	True	$\langle \chi^1, \chi^2, \chi^3 \rangle$	–
χ^4	\emptyset	$\{1, 2, 3\}$	$\mathbf{B} \cup \{4\}$	False	$\langle \chi^1, \chi^2, \chi^3 \rangle$	$\langle \chi^4 \rangle$
χ^5	$\{4\}$	$\{1, 2, 3\}$	$\mathbf{B} \cup \{5\}$	False	$\langle \chi^1, \chi^2, \chi^3 \rangle$	$\langle \chi^4, \chi^5 \rangle$
χ^6	$\{4, 5\}$	$\{1, 2, 3\}$	$\mathbf{B} \cup \{6\}$	True	$\langle \chi^1, \chi^2, \chi^3, \chi^6 \rangle$	$\langle \chi^4, \chi^5 \rangle$
χ^7	$\{4, 5\}$	$\{1, 2, 3, 6\}$	$\mathbf{B} \cup \{7\}$	True	$\langle \chi^1, \chi^2, \chi^3, \chi^6, \chi^7 \rangle$	$\langle \chi^4, \chi^5 \rangle$
χ^8	$\{4, 5\}$	$\{1, 2, 3, 6, 7\}$	$\mathbf{B} \cup \{8\}$	False	$\langle \chi^1, \chi^2, \chi^3, \chi^6, \chi^7 \rangle$	$\langle \chi^4, \chi^5, \chi^8 \rangle$
χ^9	$\{4, 5, 8\}$	$\{1, 2, 3, 6, 7\}$	$\mathbf{B} \cup \{9\}$	True	$\langle \chi^1, \chi^2, \chi^3, \chi^6, \chi^7, \chi^9 \rangle$	$\langle \chi^4, \chi^5, \chi^8 \rangle$

The post-condition remains the same. Suppose the reasoner returns True again – we then add χ^2 to \mathbf{x}^B (Figure 3, top middle). Following similar steps, we add χ^3 to \mathbf{x}^B (Figure 3, top right). When it comes to χ^4 , we allow ϵ -perturbations for $\langle \chi^1, \chi^2, \chi^3, \chi^4 \rangle$ while the other features are fixed. Suppose this time the reasoner returns False – there exists a counterexample (this counterexample is the counterfactual for feature χ^4) that violates $\mathcal{N}(\mathbf{x}) = \mathcal{N}(\hat{\mathbf{x}})$, i.e., the prediction can be different. Then, according to Equation (2) of Definition 2.1, we add χ^4 to the optimal explanation \mathbf{x}^A (shown as green in Figure 3, middle left). The computation continues until all the input features are visited. Eventually, we have $\mathbf{x}^A = \langle \chi^4, \chi^5, \chi^8 \rangle$ (Figure 3, bottom right), which means that, if the features in the explanation are fixed, the model’s prediction is invariant to any ϵ -perturbation on the other features. Additionally, for each of the features in \mathbf{x}^A , we have a counterfactual explanation that demonstrates how that feature can be altered (together with irrelevant features) to change the prediction.

3.1. Building Optimal Robust Explanations and Counterfactuals Iteratively

We now formally describe our VERIX methodology, which exploits an automated reasoning engine for neural network verification as a black-box sub-procedure. We assume the reasoner takes as inputs a network \mathcal{N} and a specification

$$\phi_{in}(\hat{\mathbf{x}}) \Rightarrow \phi_{out}(\hat{c}) \quad (3)$$

where $\hat{\mathbf{x}}$ are variables representing the network inputs and \hat{c} are expressions representing the network outputs. $\phi_{in}(\hat{\mathbf{x}})$ and $\phi_{out}(\hat{c})$ are formulas. We use $\hat{\chi}^i$ to denote the variable corresponding to the i^{th} feature. The reasoner checks whether a specification holds on a network.

As shown in Algorithm 1, the VERIX procedure takes as input a network \mathcal{N} and an input $\mathbf{x} = \langle \chi^1, \dots, \chi^d \rangle$. It outputs an optimal explanation \mathbf{x}^A with respect to perturbation magnitude ϵ , distance metric p , and discrepancy δ . It also outputs a set of counterfactual explanations, one for each feature in \mathbf{x}^A . The procedure maintains three sets, **A**, **B**, and **C**,

Algorithm 1 VERIX (VERified explainability)

Input: neural network \mathcal{N} and input $\mathbf{x} = \langle \chi^1, \dots, \chi^d \rangle$
Parameter: ϵ -perturbation, norm p , and discrepancy δ
Output: optimal robust explanation \mathbf{x}^A , counterfactuals **C** for each $\chi \in \mathbf{x}^A$

- 1: **function** VERIX(\mathcal{N}, \mathbf{x})
- 2: **A**, **B**, **C** $\mapsto \emptyset, \emptyset, \emptyset$
- 3: $c \mapsto \mathcal{N}(\mathbf{x})$
- 4: $\hat{c} \mapsto \mathcal{N}(\hat{\mathbf{x}})$
- 5: $\pi \mapsto \text{TRAVERSALORDER}(\mathbf{x})$
- 6: **for** i in π **do**
- 7: $\mathbf{B}' \mapsto \mathbf{B} \cup \{i\}$
- 8: $\phi \mapsto (\|\hat{\chi}^{\mathbf{B}'} - \chi^{\mathbf{B}'}\|_p \leq \epsilon)$
- 9: $\phi \mapsto \phi \wedge (\hat{\chi}^{\Theta \setminus \mathbf{B}'} = \chi^{\Theta \setminus \mathbf{B}'})$
- 10: (HOLD, m) $\mapsto \text{CHECK}(\mathcal{N}, \phi \Rightarrow |\hat{c} - c| \leq \delta)$
- 11: **if** HOLD **then** $\mathbf{B} \mapsto \mathbf{B}'$
- 12: **else** $\mathbf{A} \mapsto \mathbf{A} \cup \{i\}$; $\mathbf{C} \mapsto \mathbf{C} \cup \{m\}$
- 13: **return** (\mathbf{x}^A, \mathbf{C})

throughout: **A** comprises feature indices forming the explanation; **B** includes feature indices that can be excluded from the explanation; and **C** is the set of counterfactual explanations. Recall that \mathbf{x}^B denotes the *irrelevant* features (i.e., perturbing \mathbf{x}^B while leaving \mathbf{x}^A unchanged never changes the prediction). To start with, these sets are initialized to \emptyset (Line 2), and the prediction for input \mathbf{x} is recorded as c , for which we remark that c may or may not be an *accurate* prediction according to the ground truth – VERIX generates an explanation regardless. Overall, the procedure examines every feature χ^i in \mathbf{x} according to TRAVERSALORDER (Line 5) to determine whether i can be added to **B** or must belong to **A**. The traversal order can significantly affect the size and shape of the explanation. We propose a heuristic for computing a traversal order that aims to produce small explanations in Section 3.3 (in Example 3.1, a sequential order is used for ease of explanation). For each i , we compute ϕ , a formula that encodes two conditions: (i) the current χ^i

and \mathbf{x}^B are allowed to be perturbed by at most ϵ (Line 8); and (ii) the rest of the features are fixed (Line 9). The property that we check is that ϕ implies $|\hat{c} - c| \leq \delta$ (Line 10), denoting prediction invariance.

An automated reasoning sub-procedure CHECK is deployed to examine whether on network \mathcal{N} the specification $\phi \Rightarrow |\hat{c} - c| \leq \delta$ holds (Line 10), i.e., whether perturbing the current χ^i and irrelevant features while fixing the rest ensures a consistent prediction. It returns (True, m) if this is the case (where m is arbitrary) and (False, m) if not, where m is a concrete input falsifying the formula. In practice, this CHECK can be instantiated with an off-the-shelf neural network verification tool (Singh et al., 2019; Müller et al., 2022; Katz et al., 2019; Wang et al., 2021b; Henriksen & Lomuscio, 2020). If HOLD is True, i is added to the irrelevant set \mathbf{B} (Line 11). Otherwise, i is added to the explanation index set \mathbf{A} (Line 12), which conceptually indicates that χ^i contributes to the explanation of the prediction (since feature indices in \mathbf{B} have already been proven to not affect prediction). In other words, an ϵ -perturbation that includes the irrelevant features as well as the current χ^i can breach the decision boundary of \mathcal{N} . This fact is represented by the counterexample m , which represents the counterfactual explanation for χ^i and is added to the set \mathbf{C} of counterfactual explanations. The procedure continues until all feature indices in \mathbf{x} are traversed and placed into one of the two disjoint sets \mathbf{A} and \mathbf{B} . At the end, \mathbf{x}^A is returned as the optimal explanation and \mathbf{C} is returned as the set of counterfactuals.

3.2. Analysis of Soundness and Optimality

To ensure the procedure returns a robust explanation, we require that CHECK is *sound*, i.e., the solver returns True only if the specification actually holds. For the robust explanation to be optimal, CHECK also needs to be *complete*, i.e., the solver always returns True if the specification holds. We can incorporate various existing reasoners as the CHECK sub-routine. We note that an incomplete reasoner (the solver may return Unknown) does *not* undermine the soundness of our approach, though it does affect optimality (the produced explanations may be larger than necessary). Below, we state these two properties, with rigorous proofs in Appendix A.

Lemma 3.2. *If CHECK is sound, at the end of each iteration in Algorithm 1, the irrelevant set of indices \mathbf{B} satisfies*

$$\left(\left\| \hat{\chi}^{\mathbf{B}'} - \chi^{\mathbf{B}'} \right\|_p \leq \epsilon \right) \wedge (\hat{\chi}^{\Theta \setminus \mathbf{B}'} = \chi^{\Theta \setminus \mathbf{B}'}) \Rightarrow |\hat{c} - c| \leq \delta.$$

Intuitively, any ϵ -perturbation imposed upon all irrelevant features when fixing the others will always keep the prediction consistent, i.e., the infinite number of input variants (indicated with a small blue “+” in Figure 2) will always remain within the decision boundary. This can be proven by induction on the number of iterations. Soundness directly follows from Lemma 3.2.

Theorem 3.3 (Soundness). *If CHECK is sound, then the value \mathbf{x}^A returned by Algorithm 1 is a robust explanation.*

Theorem 3.4 (Optimality). *If CHECK is sound and complete, then the robust explanation \mathbf{x}^A returned by Algorithm 1 is optimal.*

Intuitively, optimality holds because if it is not possible for an ϵ -perturbation on some feature χ^i in explanation \mathbf{x}^A to change the prediction, then it will be added to the irrelevant features \mathbf{x}^B when feature χ^i is considered during the execution of Algorithm 1.

Proposition 3.5 (Complexity). *Given a d -dimensional input \mathbf{x} and a network \mathcal{N} , the complexity of computing an optimal robust explanation using the VERIX algorithm is $O(d \cdot P(\mathcal{N}))$, where $P(\mathcal{N})$ is the cost of checking a specification (as in Equation (3)) over \mathcal{N} .*

An optimal explanation can be achieved from one traversal of input features. If \mathcal{N} is piecewise-linear, checking a specification over \mathcal{N} is NP-complete (Katz et al., 2017).

3.3. Feature-Level Sensitivity Traversal

Example 3.1 used a straightforward left-to-right and top-to-bottom traversal order. Here we introduce a heuristic based on *feature-level sensitivity*, inspired by the occlusion method (Zeiler & Fergus, 2014).

Definition 3.6 (Feature-Level Sensitivity). Given an input $\mathbf{x} = \langle \chi^1, \dots, \chi^d \rangle$ and a network \mathcal{N} , the feature-level *sensitivity* (in classification for a label c or in regression for a single quantity) for a feature χ^i with respect to a transformation \mathcal{T} is

$$\text{sensitivity}(\chi^i) = \mathcal{N}_{(c)}(\mathbf{x}) - \mathcal{N}_{(c)}(\mathbf{x}'), \quad (4)$$

where \mathbf{x}' is \mathbf{x} with χ^i replaced by $\mathcal{T}(\chi^i)$.

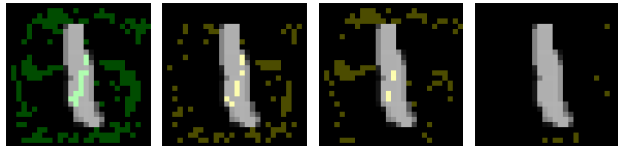
Typical transformations include *deletion* ($\mathcal{T}(\chi) = 0$) and *reversal* ($\mathcal{T}(\chi) = \bar{\chi} - \chi$, where $\bar{\chi}$ is the maximum value for feature χ). Intuitively, we measure how sensitive (in terms of an increase or decrease) a model’s confidence is to each individual feature. Given sensitivity values with respect to some transformation, we rank the feature indices into a traversal order from least sensitive to most sensitive.

4. Experimental Results

We have implemented the VERIX algorithm in Python, using the Marabou (Katz et al., 2019) neural network verification tool to implement CHECK (Algorithm 1, Line 10). Marabou’s Python API supports specification encoding and incremental solving, making it a good fit. We trained fully-connected and convolutional networks on the MNIST (LeCun et al., 2010), GTSRB (Stallkamp et al., 2012), and TaxiNet (Julian et al., 2020) datasets for classification and



(a) “keep right”, “50 mph”, “road work”, “no passing”



(b) “1”, not “8”, not “5”, not “2”

Figure 4. Optimal robust explanations (green) from VERIX on GTSRB (top) and MNIST (bottom) images. (b) Pixels in yellow are those in the explanation to rule out different counterfactuals.


 (a) MNIST “0” (b) $\epsilon : 100\% \rightarrow 10\%$ (c) $\epsilon : 100\% \rightarrow 5\%$

Figure 5. Visualization of the expansion of the irrelevant pixels when perturbation magnitude ϵ decreases from 100% to 10% and further to 5% (from deep blue to light yellow). Each brighter color denotes the pixels added when moving to the next smaller ϵ , e.g., 100%, 90%, 80% and so on.

regression tasks. Model specifications are in Appendix D. Experiments were performed on a cluster equipped with Intel Xeon E5-2637 v4 CPUs running Ubuntu 16.04. We set a time limit of 300 seconds for each CHECK call.

4.1. Example Explanations

Figure 4 shows examples of VERIX explanations for GTSRB and MNIST images. The convolutional model trained on GTSRB and fully-connected model on MNIST are in Appendix D, Tables 7 and 5. Aligning with our intuition, VERIX can distinguish the traffic signs (no matter a circle, a triangle, or a square in Figure 9a) from their surroundings well; the explanations focus on the actual contents within the signs, e.g., the right arrow denoting “keep right” and the number 50 as in “50 mph”. Interestingly, for traffic signs consisting of irregular dark shapes on a white background such as “road work” and “no passing”, VERIX discovers that the white background contains the essential features. We observe that MNIST explanations are in general more scattered around the background because the network relies on the non-existence of white pixels to rule out different counterfactuals (Figure 4b shows which pixels in the explanation have associated counterfactuals with predictions of “8”, “5”, and “2”, respectively), whereas GTSRB explana-



(a) “keep right”, VERIX, Anchors, segmentation



(b) “keep right”, VERIX, Anchors, misclassified example

Figure 6. Comparing VERIX (green) to Anchors (red) on two versions of a “keep right” traffic sign, one with strong light in the background and one without.

Table 2. VERIX vs. Anchors regarding average explanation size (number of pixels) and generation time (seconds). In VERIX, ϵ is set to 5% for MNIST and 0.5% for GTSRB.

	MNIST		GTSRB	
	size	time	size	time
VERIX (sensitivity)	180.6	174.77	357.0	853.91
VERIX (random)	294.2	157.47	383.5	814.18
Anchors	494.9	13.46	557.7	26.15

tions can safely disregard the surrounding pixels outside the traffic signs.

4.2. Effect of Varying ϵ -Perturbations

A key parameter of VERIX is the perturbation magnitude ϵ . When ϵ is varied, the irrelevant features change accordingly. Figure 5 visualizes this, showing how the irrelevant features change when ϵ is tightened from 100% to 10% and further to 5%. As ϵ decreases, more pixels become irrelevant. Intuitively, the VERIX explanation helps reveal how the network classifies this image as “0”. The deep blue pixels are those that are irrelevant with $\epsilon = 100\%$. Light blue pixels are more sensitive, allowing perturbations of only 10%. The light yellow pixels represent 5%, and bright yellow are pixels that cannot even be perturbed 5% without changing the prediction. The resulting pattern is roughly consistent with our intuition, as the shape of the “0” can be seen embedded in the explanation.

We remark that determining a suitable magnitude ϵ is non-trivial because if ϵ is too loose, explanations may be too conservative, allowing very few pixels to change. On the other hand, if ϵ is too small, nearly the whole set of pixels could become irrelevant. For instance, in Figure 5, if we set ϵ to 1% then all pixels become irrelevant – the classifier’s prediction is robust to 1%-perturbations. The “color map” we propose makes it possible to visualize not only the explanation but also how it varies with ϵ . The user then has the

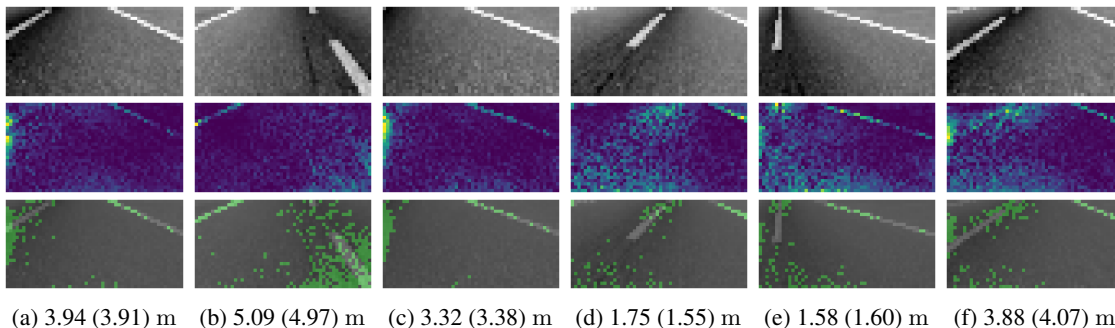


Figure 7. VERIX applied to the TaxiNet dataset – each column includes a sampled camera view (top), its sensitivity (middle), an *optimal robust explanation* (bottom), and the cross-track estimate in meters of the form “actual (estimate) m”.

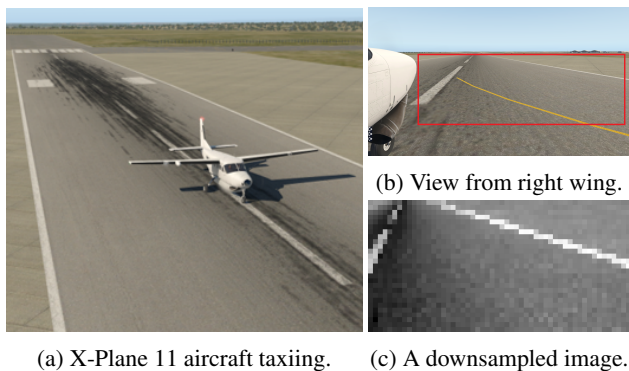


Figure 8. An autonomous aircraft taxiing scenario (Julian et al., 2020). Pictures taken from the camera fixed on the right wing are cropped (red box) and downsampled to obtain the TaxiNet dataset.

freedom to pick a specific ϵ depending on their application.

4.3. VERIX vs. Anchors

We compare VERIX with Anchors (Ribeiro et al., 2018). Figure 6 shows both approaches applied to two different versions of a “keep right” traffic sign. Anchors performs image segmentation and selects a set of the segments as the explanation, making its explanations heavily dependent on the quality of the segmentation. For instance, distractions such as strong light in the background may compromise the segments (Figure 6a, last column) thus resulting in less-than-ideal explanations, e.g., the top right region of the anchor (red) is outside the actual traffic sign. As described above, VERIX utilizes the model to compute the sensitivity traversal, often leading to more reasonable explanations. Anchors is also not designed to provide *formal* guarantees. In fact, replacing the background of an anchor explanation, which is used by (Ribeiro et al., 2018) to justify “almost” guarantee, can change the classification. For example, the last column of Figure 6b is classified as “yield” with confidence 99.92%.

Two key metrics for evaluating the quality of an explanation are the *size* and the *generation time*. Table 2 shows that overall, VERIX produces much smaller explanations than Anchors. On the other hand, it takes much longer to perform the computation necessary to ensure formal guarantees.

The two techniques thus provide a trade-off between time and explanation quality. Meanwhile, Table 2 also shows that sensitivity traversal produces significantly smaller sizes than its random counterpart with only a modest overhead in time. Due to space constraints, we include the comparison between *sensitivity* and *random* traversals in Appendix B.1.

4.4. Vision-Based Autonomous Aircraft Taxiing

We also applied VERIX to the real-world safety-critical aircraft taxiing scenario (Julian et al., 2020) shown in Figure 8. The vision-based autonomous taxiing system needs to make sure the aircraft stays on the taxiway utilizing only pictures taken from the camera on the right wing. The task is to evaluate the cross-track position of the aircraft so that a controller can adjust its position accordingly. To achieve this, a regression model is used that takes a picture as input and produces an estimate of the current position. A preprocessing step crops out the sky and aircraft nose, keeping the crucial taxiway region (in the red box). This is then downsampled into a gray-scale image of size 27×54 pixels. We label each image with its corresponding lateral distance to the runway centerline together with the taxiway heading angle. We trained a fully-connected regression network on this dataset, referred to as the TaxiNet model (Appendix D.3, Table 9), to predict the aircraft’s cross-track distance.

Figure 7 exhibits VERIX applied to the TaxiNet dataset, including a variety of taxiway images with different heading angles and number of lanes. For each taxiway, we show its VERIX explanation accompanied by a sensitivity heatmap and the cross-track estimate. We observe that the model is capable of detecting the more remote line – its contour is clearly marked in green. Meanwhile, the model is mainly focused on the centerline (especially in Figures 7b, 7d, 7e, and 7f), which makes sense as it needs to measure how far the aircraft has deviated from the center. Interestingly, while we intuitively might assume that the model would focus on the white lanes and discard the rest, VERIX shows that the bottom middle region is also crucial to the explanation (e.g., as shown in Figures 7a and 7c). This is because the model must take into account the presence and absence of the

Table 3. Average execution time (seconds) of CHECK and VERIX for *complete* verification. In particular, magnitude ϵ is set to 3% across the Dense, Dense (large), CNN models and the MNIST, TaxiNet, GTSRB datasets for sensible comparison.

	Dense		Dense (large)		CNN	
	CHECK	VERIX	CHECK	VERIX	CHECK	VERIX
MNIST (28 × 28)	0.013	160.59	0.055	615.85	0.484	4956.91
TaxiNet (27 × 54)	0.020	114.69	0.085	386.62	2.609	8814.85
GTSRB (32 × 32 × 3)	0.091	675.04	0.257	1829.91	1.574	12935.27

Table 4. Average execution time (seconds) of CHECK and VERIX for *incomplete* verification. Magnitude ϵ is 3% for both MNIST-sota and GTSRB-sota models.

	# ReLU	# MaxPool	CHECK	VERIX
MNIST-sota	50960	5632	2.31	1841.25
GTSRB-sota	106416	5632	8.54	8770.15

centerline. This is in fact in consistent with our observations about the black background in MNIST images (Figure 1). We used $\epsilon = 5\%$ for these explanations, which suggests that for modest perturbations (e.g., brightness change due to different weather conditions) the predicted cross-track estimate will remain within an acceptable discrepancy, and taxiing will not be compromised.

4.5. Runtime Performance

We analyze the empirical time *complexity* of our VERIX approach in Table 3. The model structures are described in Appendix D.4. Typically, the individual pixel checks (CHECK) return a definitive answer (True or False) within a second on dense models and in a few seconds on convolutional networks. For image benchmarks such as MNIST and GTSRB, larger inputs or more complicated models result in longer (pixel- and image-level) execution times for generating explanations. As for TaxiNet as a regression task, while its pixel-level check takes longer than that of MNIST, it is actually faster in total time on dense models because TaxiNet does not need to check against other labels.

The *scalability* of VERIX can be improved if we perform incomplete verification, for which we re-emphasize that the soundness of the resulting explanations is not undermined. To illustrate, we deploy the incomplete CROWN (Zhang et al., 2018) analysis (implemented in Marabou) to perform the CHECK sub-procedure. Table 4 reports the runtime performance of VERIX when using incomplete verification on state-of-the-art network architectures with hundreds of thousands of neurons. See models in Appendix D, Tables 6 and 8. In general, the scalability of VERIX will grow with that of verification tools, which has improved significantly in the past several years as demonstrated by the results from the Verification of Neural Networks Competitions (VNN-COMP) (Bak et al., 2022).

5. Related Work

Earlier work on formal explanations (Marques-Silva & Ignatiev, 2022) has the following limitations. First, in terms of *scalability*, they can only handle simple machine learning models such as naive Bayes classifiers (Marques-Silva et al., 2020), random forests (Izza & Marques-Silva, 2021; Boumazouza et al., 2021), decision trees (Izza et al., 2022), and boosted trees (Ignatiev, 2020; Ignatiev et al., 2022). In particular, (Ignatiev et al., 2019) addresses networks but with very simple structure (e.g., one hidden layer of 15 or 20 neurons trained to distinguish two MNIST digits). In contrast, VERIX works with networks applicable to real-world safety-critical scenarios. Second, the *size* of explanations can be unnecessarily large. As a workaround, approximate explanations (Waeldchen et al., 2021; Wang et al., 2021a) are proposed as a generalization to provide probabilistic (thus compromised) guarantees of prediction invariance. VERIX, by using feature-level sensitivity ranking, produces reasonably-sized explanations with rigorous guarantees. Third, these formal explanations allow *any possible input* in feature space, which is not necessary or realistic. (La Malfa et al., 2021) introduces two *bounded* perturbations for NLP models, *k*-NN box closure and ϵ -ball. Our approach is essentially an extension of this work as described earlier. Note that a direct comparison with (La Malfa et al., 2021) would not be meaningful as they only handle NLP models, and adapting their technique to perception models is one of our contributions.

Due to space constraints, we include the related work on verification of neural networks in Appendix C.1.

6. Conclusions and Future Work

We have presented the VERIX framework for computing optimal robust explanations and counterfactuals along the decision boundary. A possible future direction is generalizing to other crucial properties such as *fairness*. Recall the loan application model in Section 1; our approach can discover potential bias (if it exists) by including those “gender” and “ethnicity” attributes in the produced explanations; then a human decision-maker can better interpret the loan prediction outcomes to promote a fair and unbiased model.

References

- Anderson, G., Pailoor, S., Dillig, I., and Chaudhuri, S. Optimization and abstraction: a synergistic approach for analyzing neural network robustness. In *Proceedings of the 40th ACM SIGPLAN Conference on Programming Language Design and Implementation*, pp. 731–744, 2019.
- Bak, S., Liu, C., Johnson, T. T., Brix, C., and Müller, M. The 3rd international verification of neural networks competition (vnn-comp), 2022. <https://sites.google.com/view/vnn2022>.
- Bassan, S. and Katz, G. Towards formal approximated minimal explanations of neural networks. *arXiv preprint arXiv:2210.13915*, 2022.
- Botoeva, E., Kouvaros, P., Kronqvist, J., Lomuscio, A., and Misener, R. Efficient verification of relu-based neural networks via dependency analysis. In *Proceedings of the AAAI Conference on Artificial Intelligence*, volume 34, pp. 3291–3299, 2020.
- Boumazouza, R., Cheikh-Alili, F., Mazure, B., and Tabia, K. Asteryx: A model-agnostic sat-based approach for symbolic and score-based explanations. In *Proceedings of the 30th ACM International Conference on Information & Knowledge Management*, pp. 120–129, 2021.
- Bunel, R., Turkaslan, I., Torr, P. H., Kumar, M. P., Lu, J., and Kohli, P. Branch and bound for piecewise linear neural network verification. *Journal of Machine Learning Research*, 21:1–39, 2020.
- Darwiche, A. and Hirth, A. On the reasons behind decisions. 2020.
- De Palma, A., Behl, H. S., Bunel, R., Torr, P., and Kumar, M. P. Scaling the convex barrier with active sets. In *International Conference on Learning Representations*, 2021.
- Ehlers, R. Formal verification of piece-wise linear feed-forward neural networks. In *International Symposium on Automated Technology for Verification and Analysis*, pp. 269–286. Springer, 2017.
- Ferrari, C., Mueller, M. N., Jovanović, N., and Vechev, M. Complete verification via multi-neuron relaxation guided branch-and-bound. In *International Conference on Learning Representations*, 2022.
- Gehr, T., Mirman, M., Drachler-Cohen, D., Tsankov, P., Chaudhuri, S., and Vechev, M. AI2: safety and robustness certification of neural networks with abstract interpretation. In *2018 IEEE symposium on security and privacy (SP)*, pp. 3–18. IEEE, 2018.
- Grigorescu, S., Trasnea, B., Cocias, T., and Macesanu, G. A survey of deep learning techniques for autonomous driving. *Journal of Field Robotics*, 37(3):362–386, 2020.
- Henriksen, P. and Lomuscio, A. Efficient neural network verification via adaptive refinement and adversarial search. In *ECAI 2020*, pp. 2513–2520. IOS Press, 2020.
- Huang, X., Kwiatkowska, M., Wang, S., and Wu, M. Safety verification of deep neural networks. In *International conference on computer aided verification*, pp. 3–29. Springer, 2017.
- Huang, X., Kroening, D., Ruan, W., Sharp, J., Sun, Y., Thamo, E., Wu, M., and Yi, X. A survey of safety and trustworthiness of deep neural networks: Verification, testing, adversarial attack and defence, and interpretability. *Computer Science Review*, 37:100270, 2020. ISSN 1574-0137. doi: <https://doi.org/10.1016/j.cosrev.2020.100270>.
- Ignatiev, A. Towards trustable explainable ai. In *Proceedings of the Twenty-Ninth International Conference on International Joint Conferences on Artificial Intelligence*, pp. 5154–5158, 2020.
- Ignatiev, A., Narodytska, N., and Marques-Silva, J. Abduction-based explanations for machine learning models. In *Proceedings of the AAAI Conference on Artificial Intelligence*, volume 33, pp. 1511–1519, 2019.
- Ignatiev, A., Izza, Y., Stuckey, P. J., and Marques-Silva, J. Using maxsat for efficient explanations of tree ensembles. In *Proceedings of the AAAI Conference on Artificial Intelligence*, volume 36, pp. 3776–3785, 2022.
- Izza, Y. and Marques-Silva, J. On explaining random forests with sat. In Zhou, Z.-H. (ed.), *Proceedings of the Thirtieth International Joint Conference on Artificial Intelligence, IJCAI-21*, pp. 2584–2591. International Joint Conferences on Artificial Intelligence Organization, 8 2021. doi: 10.24963/ijcai.2021/356. Main Track.
- Izza, Y., Ignatiev, A., and Marques-Silva, J. On tackling explanation redundancy in decision trees. *J. Artif. Intell. Res.*, 75:261–321, 2022. doi: 10.1613/jair.1.13575.
- Julian, K. D., Lee, R., and Kochenderfer, M. J. Validation of image-based neural network controllers through adaptive stress testing. In *2020 IEEE 23rd international conference on intelligent transportation systems (ITSC)*, pp. 1–7. IEEE, 2020.
- Katz, G., Barrett, C., Dill, D. L., Julian, K., and Kochenderfer, M. J. Reluplex: An efficient smt solver for verifying deep neural networks. In *International Conference on Computer Aided Verification*, pp. 97–117. Springer, 2017.

- Katz, G., Huang, D. A., Ibeling, D., Julian, K., Lazarus, C., Lim, R., Shah, P., Thakoor, S., Wu, H., Zeljić, A., et al. The marabou framework for verification and analysis of deep neural networks. In *International Conference on Computer Aided Verification*, pp. 443–452, 2019.
- Khedr, H., Ferlez, J., and Shoukry, Y. Peregrinn: Penalized-relaxation greedy neural network verifier. In *International Conference on Computer Aided Verification*, pp. 287–300. Springer, 2021.
- La Malfa, E., Michelmore, R., Zbrzezny, A. M., Paoletti, N., and Kwiatkowska, M. On guaranteed optimal robust explanations for nlp models. In Zhou, Z.-H. (ed.), *Proceedings of the Thirtieth International Joint Conference on Artificial Intelligence, IJCAI-21*, pp. 2658–2665. International Joint Conferences on Artificial Intelligence Organization, 8 2021. doi: 10.24963/ijcai.2021/366.
- LeCun, Y., Cortes, C., and Burges, C. Mnist handwritten digit database. *ATT Labs [Online]*. Available: <http://yann.lecun.com/exdb/mnist>, 2, 2010.
- Liu, C., Arnon, T., Lazarus, C., Strong, C., Barrett, C., Kochenderfer, M. J., et al. Algorithms for verifying deep neural networks. *Foundations and Trends® in Optimization*, 4(3-4):244–404, 2021.
- Lloyd, S. Least squares quantization in pcm. *IEEE transactions on information theory*, 28(2):129–137, 1982.
- Lundberg, S. M. and Lee, S.-I. A unified approach to interpreting model predictions. In *Proceedings of the 31st International Conference on Neural Information Processing Systems*, pp. 4768–4777, 2017.
- Marques-Silva, J. and Ignatiev, A. Delivering trustworthy ai through formal xai. In *Proceedings of the AAAI Conference on Artificial Intelligence*, pp. 3806–3814, 2022.
- Marques-Silva, J., Gerspacher, T., Cooper, M. C., Ignatiev, A., and Narodytska, N. Explaining naive bayes and other linear classifiers with polynomial time and delay. In *Proceedings of the 34th International Conference on Neural Information Processing Systems*, pp. 20590–20600, 2020.
- Müller, M. N., Makarchuk, G., Singh, G., Püschel, M., and Vechev, M. Prima: general and precise neural network certification via scalable convex hull approximations. *Proceedings of the ACM on Programming Languages*, 6(POPL):1–33, 2022.
- Ribeiro, M. T., Singh, S., and Guestrin, C. “why should i trust you?” explaining the predictions of any classifier. In *Proceedings of the 22nd ACM SIGKDD international conference on knowledge discovery and data mining*, pp. 1135–1144, 2016.
- Ribeiro, M. T., Singh, S., and Guestrin, C. Anchors: high-precision model-agnostic explanations. In *Proceedings of the Thirty-Second AAAI Conference on Artificial Intelligence and Thirtieth Innovative Applications of Artificial Intelligence Conference and Eighth AAAI Symposium on Educational Advances in Artificial Intelligence*, pp. 1527–1535, 2018.
- Ruan, W., Wu, M., Sun, Y., Huang, X., Kroening, D., and Kwiatkowska, M. Global robustness evaluation of deep neural networks with provable guarantees for the Hamming distance. In *Proceedings of the Twenty-Eighth International Joint Conference on Artificial Intelligence, IJCAI-19*, pp. 5944–5952, 7 2019. doi: 10.24963/ijcai.2019/824.
- Shih, A., Choi, A., and Darwiche, A. A symbolic approach to explaining bayesian network classifiers. In *Proceedings of the 27th International Joint Conference on Artificial Intelligence*, pp. 5103–5111, 2018.
- Singh, G., Gehr, T., Püschel, M., and Vechev, M. An abstract domain for certifying neural networks. *Proceedings of the ACM on Programming Languages*, 3(POPL):1–30, 2019.
- Stallkamp, J., Schlipsing, M., Salmen, J., and Igel, C. Man vs. computer: Benchmarking machine learning algorithms for traffic sign recognition. *Neural networks*, 32: 323–332, 2012.
- Tjeng, V., Xiao, K. Y., and Tedrake, R. Evaluating robustness of neural networks with mixed integer programming. In *International Conference on Learning Representations*, 2019.
- Tran, H.-D., Bak, S., Xiang, W., and Johnson, T. T. Verification of deep convolutional neural networks using imagestars. In *International Conference on Computer Aided Verification*, pp. 18–42. Springer, 2020.
- Verma, S., Boonsanong, V., Hoang, M., Hines, K. E., Dickerson, J. P., and Shah, C. Counterfactual explanations and algorithmic recourses for machine learning: A review. *arXiv preprint arXiv:2010.10596*, 2020.
- Wachter, S., Mittelstadt, B., and Russell, C. Counterfactual explanations without opening the black box: Automated decisions and the gdpr. *Harvard Journal of Law & Technology*, 31(2):2018, 2017.
- Waeldechen, S., Macdonald, J., Hauch, S., and Kutyniok, G. The computational complexity of understanding binary classifier decisions. *Journal of Artificial Intelligence Research*, 70:351–387, 2021.

- Wang, E., Khosravi, P., and Van den Broeck, G. Probabilistic sufficient explanations. In Zhou, Z.-H. (ed.), *Proceedings of the Thirtieth International Joint Conference on Artificial Intelligence, IJCAI-21*, pp. 3082–3088. International Joint Conferences on Artificial Intelligence Organization, 8 2021a. doi: 10.24963/ijcai.2021/424. Main Track.
- Wang, S., Pei, K., Whitehouse, J., Yang, J., and Jana, S. Efficient formal safety analysis of neural networks. In *Proceedings of the 32nd International Conference on Neural Information Processing Systems*, pp. 6369–6379, 2018a.
- Wang, S., Pei, K., Whitehouse, J., Yang, J., and Jana, S. Formal security analysis of neural networks using symbolic intervals. In *Proceedings of the 27th USENIX Conference on Security Symposium*, pp. 1599–1614, 2018b.
- Wang, S., Zhang, H., Xu, K., Lin, X., Jana, S., Hsieh, C.-J., and Kolter, Z. Beta-crown: Efficient bound propagation with per-neuron split constraints for neural network robustness verification. In *Proceedings of the 35th Conference on Neural Information Processing Systems (NeurIPS)*, volume 34, pp. 29909–29921, 2021b.
- Wu, H., Ozdemir, A., Zeljić, A., Julian, K., Irfan, A., Gopinath, D., Fouladi, S., Katz, G., Pasareanu, C., and Barrett, C. Parallelization techniques for verifying neural networks. In *2020 Formal Methods in Computer Aided Design (FMCAD)*, pp. 128–137. IEEE, 2020a.
- Wu, H., Barrett, C., Sharif, M., Narodytska, N., and Singh, G. Scalable verification of GNN-based job schedulers. *Proc. ACM Program. Lang.*, 6(OOPSLA2), oct 2022a. doi: 10.1145/3563325.
- Wu, H., Zeljić, A., Katz, G., and Barrett, C. Efficient neural network analysis with sum-of-infeasibilities. In *International Conference on Tools and Algorithms for the Construction and Analysis of Systems*, pp. 143–163. Springer, 2022b.
- Wu, H., Tagomori, T., Robey, A., Yang, F., Matni, N., Pappas, G., Hassani, H., Pasareanu, C., and Barrett, C. Toward certified robustness against real-world distribution shifts. In *IEEE Conference on Secure and Trustworthy Machine Learning*, 2023.
- Wu, M. and Kwiatkowska, M. Robustness guarantees for deep neural networks on videos. In *Proceedings of the IEEE/CVF Conference on Computer Vision and Pattern Recognition*, pp. 311–320, 2020.
- Wu, M., Wicker, M., Ruan, W., Huang, X., and Kwiatkowska, M. A game-based approximate verification of deep neural networks with provable guarantees. *Theoretical Computer Science*, 807:298–329, 2020b.
- Yu, K.-H., Beam, A. L., and Kohane, I. S. Artificial intelligence in healthcare. *Nature biomedical engineering*, 2 (10):719–731, 2018.
- Zeiler, M. D. and Fergus, R. Visualizing and understanding convolutional networks. In *European conference on computer vision*, pp. 818–833. Springer, 2014.
- Zelazny, T., Wu, H., Barrett, C., and Katz, G. On optimizing back-substitution methods for neural network verification. In *Formal Methods in Computer Aided Design (FMCAD)*, pp. 17–26. IEEE, 2022.
- Zhang, H., Weng, T.-W., Chen, P.-Y., Hsieh, C.-J., and Daniel, L. Efficient neural network robustness certification with general activation functions. In *Proceedings of the 32nd International Conference on Neural Information Processing Systems*, pp. 4944–4953, 2018.

A. Proofs for Theorems

We present rigorous proofs for Lemma 3.2, Theorems 3.3 and 3.4 in Section 3.1, justifying the *soundness* and *optimality* of our VERIX approach. For better readability, we repeat each lemma and theorem before their corresponding proofs.

A.1. Proof for Lemma 3.2

Lemma 3.2. If CHECK is sound, at the end of each iteration in Algorithm 1, the *irrelevant* set of indices \mathbf{B} satisfies

$$\left(\|\hat{\chi}^{\mathbf{B}'} - \chi^{\mathbf{B}'}\|_p \leq \epsilon\right) \wedge (\hat{\chi}^{\Theta \setminus \mathbf{B}'} = \chi^{\Theta \setminus \mathbf{B}'}) \Rightarrow |\hat{c} - c| \leq \delta.$$

Proof. Recall that the sub-procedure CHECK is sound means the deployed automated reasoner returns True only if the specification actually holds. That is, from Line 10 we have

$$\phi \Rightarrow |\hat{c} - c| \leq \delta$$

holds on network \mathcal{N} . Simultaneously, from Lines 8 and 9 we know that, to check the current feature χ^i of the traversing order π , the pre-condition ϕ contains

$$\phi \mapsto \left(\|\hat{\chi}^{\mathbf{B}'} - \chi^{\mathbf{B}'}\|_p \leq \epsilon\right) \wedge (\hat{\chi}^{\Theta \setminus \mathbf{B}'} = \chi^{\Theta \setminus \mathbf{B}'}).$$

Specifically, we prove this through induction on the number of iteration i . When i is 0, pre-condition ϕ is initialised as \top and the specification holds trivially. In the inductive case, suppose CHECK returns False, then the set \mathbf{B} is unchanged as in Line 12. Otherwise, if CHECK returns True, which makes HOLD become True, then the current feature index i is added into the irrelevant set of feature indices \mathbf{B} as in Line 11, with such satisfying specification

$$\left(\|\hat{\chi}^{\mathbf{B}'} - \chi^{\mathbf{B}'}\|_p \leq \epsilon\right) \wedge (\hat{\chi}^{\Theta \setminus \mathbf{B}'} = \chi^{\Theta \setminus \mathbf{B}'}) \Rightarrow |\hat{c} - c| \leq \delta.$$

As the iteration proceeds, each time CHECK returns True, the irrelevant set \mathbf{B} is augmented with the current feature index i , and the specification always holds as it is explicitly checked by the CHECK reasoner. \square

A.2. Proof for Theorem 3.3

Theorem 3.3 (Soundness). If CHECK is sound, then the value $\mathbf{x}^{\mathbf{A}}$ returned by Algorithm 1 is a *robust* explanation.

Proof. The for-loop from Line 6 indicates that Algorithm 1 goes through every each feature \mathbf{x}^i in input \mathbf{x} by traversing the set of indices $\Theta(\mathbf{x})$. Line 5 means that π is one such instance of ordered traverse. When the iteration ends, all the indices in $\Theta(\mathbf{x})$ are either put into the irrelevant set of indices by $\mathbf{B} \mapsto \mathbf{B}'$ as in Line 11 or the explanation index set by $\mathbf{A} \mapsto \mathbf{A} \cup \{i\}$ as in Line 12. That is, \mathbf{A} and \mathbf{B} are two disjoint index sets forming $\Theta(\mathbf{x})$; in other words, $\mathbf{B} = \Theta(\mathbf{x}) \setminus \mathbf{A}$. Therefore, combined with Lemma 3.2, when the reasoner CHECK is sound, once iteration finishes we have the following specification

$$\left(\|\hat{\chi}^{\mathbf{B}} - \chi^{\mathbf{B}}\|_p \leq \epsilon\right) \wedge (\hat{\chi}^{\Theta \setminus \mathbf{B}} = \chi^{\Theta \setminus \mathbf{B}}) \Rightarrow |\hat{c} - c| \leq \delta.$$

holds on network \mathcal{N} , where $\hat{\chi}^{\mathbf{B}}$ is the variable representing all the possible assignments of irrelevant features $\mathbf{x}^{\mathbf{B}}$, i.e., $\forall \mathbf{x}^{\mathbf{B}'}$, and the pre-condition $\hat{\chi}^{\Theta \setminus \mathbf{B}} = \chi^{\Theta \setminus \mathbf{B}}$ fixes the values of the explanation features of an instantiated input \mathbf{x} . Meanwhile, the post-condition $|\hat{c} - c| \leq \delta$ where $c \mapsto \mathcal{N}(\mathbf{x})$ as in Line 4 ensures prediction invariance such that δ is 0 for classification and otherwise a pre-defined allowable amount of perturbation for regression. To this end, for some specific input \mathbf{x} we have the following property

$$\forall \mathbf{x}^{\mathbf{B}'}, \left(\|\mathbf{x}^{\mathbf{B}'} - \mathbf{x}^{\mathbf{B}}\|_p \leq \epsilon\right) \Rightarrow |\mathcal{N}(\mathbf{x}') - \mathcal{N}(\mathbf{x})| \leq \delta.$$

holds. Here we prove by construction. According to Equation (1) of Definition 2.1, if the irrelevant features $\mathbf{x}^{\mathbf{B}}$ satisfy the above property, then we call the rest features $\mathbf{x}^{\mathbf{A}}$ a *robust* explanation with respect to network \mathcal{N} and input \mathbf{x} . \square

A.3. Proof for Theorem 3.4

Theorem 3.4 (Optimality). If CHECK is sound and complete, then the robust explanation \mathbf{x}^A returned by Algorithm 1 is optimal.

Proof. We prove this by contradiction. From Equation (2) of Definition 2.1, we know that explanation \mathbf{x}^A is optimal if, for any feature χ in explanation, there always exists an ϵ -perturbation on χ and the irrelevant features \mathbf{x}^B such that the prediction alters. Let us suppose \mathbf{x}^A is not optimal, then there exists a feature χ in \mathbf{x}^A such that no matter how to manipulate this feature χ' and the irrelevant features $\mathbf{x}^{B'}$, the prediction always remains the same. That is,

$$\forall \mathbf{x}^{B'}, \chi', \left\| (\mathbf{x}^B \oplus \chi) - (\mathbf{x}^{B'} \oplus \chi') \right\|_p \leq \epsilon \Rightarrow |\mathcal{N}(\mathbf{x}) - \mathcal{N}(\mathbf{x}')| \leq \delta,$$

where \oplus denotes concatenation of two features. When we pass this input \mathbf{x} and network \mathcal{N} into the VERIX framework, suppose Algorithm 1 examines feature χ at the i th iteration, then as in Line 7, the current irrelevant set of indices is $\mathbf{B}' \mapsto \mathbf{B} \cup \{i\}$, and accordingly the pre-conditions are

$$\phi \mapsto \left(\left\| \hat{\chi}^{\mathbf{B} \cup \{i\}} - \chi^{\mathbf{B} \cup \{i\}} \right\|_p \leq \epsilon \right) \wedge (\hat{\chi}^{\Theta \setminus (\mathbf{B} \cup \{i\})} = \chi^{\Theta \setminus (\mathbf{B} \cup \{i\})}).$$

Because $\hat{\chi}^{\mathbf{B} \cup \{i\}}$ is the variable representing all the possible assignments of irrelevant features \mathbf{x}^B and the i th feature χ , i.e., $\forall \mathbf{x}^{B'}, \chi'$, and meanwhile

$$\hat{\chi}^{\Theta \setminus (\mathbf{B} \cup \{i\})} = \chi^{\Theta \setminus (\mathbf{B} \cup \{i\})}$$

indicates that the other features are fixed with specific values of this \mathbf{x} . Thus, with $c \mapsto \mathcal{N}(\mathbf{x})$ in Line 4, we have the specification $\phi \Rightarrow |\hat{c} - c| \leq \delta$ holds on input \mathbf{x} and network \mathcal{N} . Therefore, if the reasoner CHECK is sound and complete,

$$\text{CHECK}(\mathcal{N}, \phi \Rightarrow |\hat{c} - c| \leq \delta)$$

will always return True. Line 10 assigns True to HOLD, and index i is then put into the irrelevant set \mathbf{B} thus feature χ in the irrelevant features \mathbf{x}^B . However, based on the assumption, feature χ is in explanation \mathbf{x}^A , so χ is in \mathbf{x}^A and \mathbf{x}^B simultaneously – a contradiction occurs. Therefore, Theorem 3.4 holds. \square

B. Supplementary Experimental Results

B.1. Sensitivity vs. Random Traversal

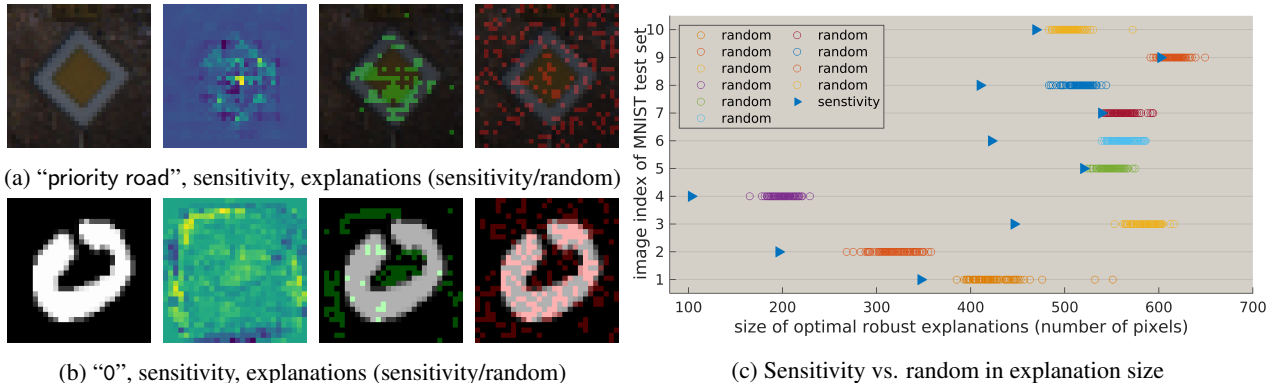


Figure 9. Comparing VERIX explanations, when using *sensitivity* (green) and random (red) traversals, on GTSRB and MNIST. (c) Each blue triangle denotes 1 deterministic explanation from sensitivity ranking, and each bunch of circles represents 100 random traversals.

To show the advantage of the *sensitivity* traversal (described in Section 3.3), Figure 9 compares VERIX explanations using sensitivity-based and random traversal orders. The first column of Figures 9a and 9b shows the original image; the second a heatmap of the sensitivity (with deletion $\mathcal{T}(\chi) = 0$ for GTSRB and reversal $\mathcal{T}(\chi) = \bar{\chi} - \chi$ for MNIST because deleting background pixels of MNIST images may contribute to little confidence change as they often have zero values); and the third and fourth columns show explanations using the sensitivity and random traversal orders, respectively. Sensitivity, as shown in the heatmaps, prioritizes pixels that have more influence on the network’s prediction. In contrast, a random ranking is simply a shuffling of all the pixels. We observe that the sensitivity traversal generates smaller and more sensible explanations. In Figure 9c, we compare explanation sizes for the first 10 images (to avoid potential selection bias) of the MNIST test set. For each image, we show 100 random traversal explanations compared to the sensitivity traversal explanation. We notice that the latter is almost always smaller, often significantly so, suggesting that sensitivity-based traversals are a reasonable heuristic for attempting to approach globally optimal explanations.

C. Supplementary Related Work

C.1. Verification of Neural Networks

Researchers have investigated how automated reasoning can aid verification of neural networks with respect to formally specified properties (Liu et al., 2021; Huang et al., 2020), by utilizing reasoners based on abstraction (Zhang et al., 2018; Singh et al., 2019; Gehr et al., 2018; Tran et al., 2020; Müller et al., 2022; Wang et al., 2018a;b; Anderson et al., 2019; Zelazny et al., 2022; Wu et al., 2022a; 2023) and search (Ehlers, 2017; Katz et al., 2017; 2019; Huang et al., 2017; Wang et al., 2021b; Tjeng et al., 2019; Henriksen & Lomuscio, 2020; Bunel et al., 2020; De Palma et al., 2021; Ruan et al., 2019; Wu et al., 2020b; Wu & Kwiatkowska, 2020; Botoeva et al., 2020; Khedr et al., 2021; Ferrari et al., 2022; Wu et al., 2020a; 2022b). Those approaches mainly focus on verifying whether a network satisfies a certain pre-defined property (e.g., robustness), i.e., either prove the property holds or disprove it with a counterexample. However, this does not shed light on *why* a network makes a specific prediction. We take a step further, repurposing those verification engines as sub-routines to inspect the decision-making process of a model, thereby explaining its behavior (through the presence or absence of certain input features). The hope is that these explanations can help humans better interpret machine learning models and thus facilitate appropriate deployment.

D. Model Specifications

Apart from those experimental settings in Section 4, we include detailed model specifications for reproducibility and reference purposes. Although evaluated on the Modified National Institute of Standards and Technology (MNIST) (LeCun et al., 2010), German Traffic Sign Recognition Benchmark (GTSRB) (Stallkamp et al., 2012), and TaxiNet (Julian et al., 2020) image datasets – MNIST and GTSRB in classification and TaxiNet in regression, our VERIX framework can be generalized to other machine learning applications such as natural language processing.

As for the sub-procedure CHECK of Algorithm 1, while VERIX can potentially incorporate existing automated reasoners, we deploy the neural network verification tool Marabou (Katz et al., 2019). While it supports various model formats such as .pb from TensorFlow and .h5 from Keras, we employ the cross platform .onnx format for better Python API support. When importing a model with softmax as the final activation function, we remark that, for the problem to be *decidable*, one needs to specify the outputName parameter of the read_onnx function as the pre-softmax logits. As a workaround for this, one can also train the model without softmax in the last layer and instead use the SoftmaxLoss loss function from the tensorflow_ranking package. Either way, VERIX produces consistent results.

D.1. MNIST

For MNIST, we train a fully-connected feed-forward neural network with 3 dense layers activated with ReLU (first 2 layers) and softmax (last classification layer) functions as in Table 5, achieving 92.26% accuracy. While the MNIST dataset can easily be trained with accuracy as high as 99.99%, we are more interested in whether a very simple model as such can extract sensible explanations – the answer is yes. Meanwhile, we also train several more complicated MNIST models, and observe that their optimal explanations share a common phenomenon such that they are relatively more scattered around the background compared to the other datasets. This cross-model observation indicates that MNIST models need to check both the presence and absence of white pixels to recognize the handwritten digits correctly. Besides, to show the scalability of VERIX, we also deploy incomplete verification on state-of-the-art model structure as in Table 6.

D.2. GTSRB

As for the GTSRB dataset, since it is not as identically distributed as MNIST, to avoid potential distribution shift, instead of training a model out of the original 43 categories, we focus on the top first 10 categories with highest occurrence in the training set. This allows us to obtain an appropriate model with high accuracy – the convolutional model we train as in Table 7 achieves a test accuracy of 93.83%. It is worth mentioning that, our convolutional model is much more complicated than the simple dense model in (Ignatiev et al., 2019), which only contains one hidden layer of 15 or 20 neurons trained to distinguish two MNIST digits. Also, as shown in Table 4 of Section 4.5, we report results on the state-of-the-art GTSRB classifier in Table 8.

D.3. TaxiNet

Apart from the classification tasks performed on those standard image recognition benchmarks, our VERIX approach can also tackle regression models, applicable to real-world safety-critical domains. In this vision-based autonomous aircraft taxiing scenario (Julian et al., 2020) of Figure 8, we train the regression model in Table 9 to produce an estimate of the cross-track distance (in meters) from the ownship to the taxiway centerline. The TaxiNet model has a mean absolute error of 0.824 on the test set, with no activation function in the last output layer.

D.4. Dense, Dense (large), and CNN

In Section 4.5, we analyze execution time of VERIX on three models with increasing complexity: Dense, Dense (large), and CNN as in Tables 10, 11, and 12, respectively. To enable a fair and sensible comparison, those three models are used across the MNIST, TaxiNet, and GTSRB datasets with only necessary adjustments to accommodate each task. For example, in all three models $h \times w \times c$ denotes different input size height \times width \times channel for each dataset. For the activation function of the last layer, softmax is used for MNIST and GTSRB while TaxiNet as a regression task needs no such activation. Finally, TaxiNet deploys he_uniform as the kernel_initializer parameter in the intermediate dense and convolutional layers for task specific reason.

Table 5. Architecture for the MNIST classifier.

Layer Type	Parameter	Activation
Input	$28 \times 28 \times 1$	–
Flatten	–	–
Fully Connected	10	ReLU
Fully Connected	10	ReLU
Fully Connected	10	softmax

Table 6. Architecture for the MNIST-sota classifier.

Type	Parameter	Activation
Input	$28 \times 28 \times 1$	–
Convolution	$3 \times 3 \times 32$	ReLU
Convolution	$3 \times 3 \times 32$	ReLU
MaxPooling	2×2	–
Convolution	$3 \times 3 \times 64$	ReLU
Convolution	$3 \times 3 \times 64$	ReLU
MaxPooling	2×2	–
Flatten	–	–
Fully Connected	200	ReLU
Dropout	0.5	–
Fully Connected	200	ReLU
Fully Connected	10	softmax

Table 7. Architecture for the GTSRB classifier.

Type	Parameter	Activation
Input	$32 \times 32 \times 3$	–
Convolution	$3 \times 3 \times 4$ (1)	–
Convolution	$2 \times 2 \times 4$ (2)	–
Fully Connected	20	ReLU
Fully Connected	10	softmax

Table 8. Architecture for the GTSRB-sota classifier.

Type	Parameter	Activation
Input	$28 \times 28 \times 1$	–
Convolution	$3 \times 3 \times 32$	ReLU
Convolution	$3 \times 3 \times 32$	ReLU
Convolution	$3 \times 3 \times 64$	ReLU
MaxPooling	2×2	–
Convolution	$3 \times 3 \times 64$	ReLU
Convolution	$3 \times 3 \times 64$	ReLU
MaxPooling	2×2	–
Flatten	–	–
Fully Connected	200	ReLU
Dropout	0.5	–
Fully Connected	200	ReLU
Fully Connected	10	softmax

Table 9. Architecture for the TaxiNet regression model.

Type	Parameter	Activation
Input	$27 \times 54 \times 1$	–
Flatten	–	–
Fully Connected	20	ReLU
Fully Connected	10	ReLU
Fully Connected	1	–

Table 10. Architecture for the Dense model.

Layer Type	Parameter	Activation
Input	$h \times w \times c$	–
Flatten	–	–
Fully Connected	10	ReLU
Fully Connected	10	ReLU
Fully Connected	10 / 1	softmax / –

Table 11. Architecture for the Dense (large) model.

Layer Type	Parameter	Activation
Input	$h \times w \times c$	–
Flatten	–	–
Fully Connected	30	ReLU
Fully Connected	30	ReLU
Fully Connected	10 / 1	softmax / –

Table 12. Architecture for the CNN model.

Layer Type	Parameter	Activation
Input	$h \times w \times c$	–
Convolution	$3 \times 3 \times 4$	–
Convolution	$3 \times 3 \times 4$	–
Fully Connected	20	ReLU
Fully Connected	10 / 1	softmax / –